# Characterization of the binding interactions between EvaGreen dye and dsDNA

L. C. T. Shoute and G. R. Loppnow*
Department of Chemistry, University of Alberta, Edmonton, AB T6G 2G2 Canada

* Corresponding Author. Email: glen.loppnow@ualberta.ca

Running Title: EvaGreen and dsDNA Binding Interactions

**ABSTRACT**

Understanding the dsDNA•EG binding interaction is important because the EvaGreen (EG) dye is increasingly used in real-time quantitative polymerase chain reaction, high resolution melting analysis, and routine quantification of DNA. In this work, a binding isotherm for the interactions of EG with duplex DNA (poly-$dA_{17}$·poly-$dT_{17}$) has been determined from the absorption and fluorescence spectra of the EG and dsDNA•EG complex. The isotherm has a sigmoidal shape and can be modeled with the Hill equation, indicating positive cooperativity for the binding interaction. A Scatchard plot of the binding data yields a concave-down curve in agreement with the Hill analysis of the binding isotherm for a positive cooperative binding interaction. Analysis of the Scatchard plot with the modified McGhee and von Hippel model for a finite one-dimensional homogeneous lattice and nonspecific binding of ligands to duplex DNA yields the intrinsic binding constant, the number of lattice sites occluded by a bound ligand, and the cooperativity parameter of 3.6 X $10^5$ $M^{-1}$, 4.0, and 8.1, respectively. The occluded site size of 4 indicates that moieties of the EG intercalate into the adjacent base pairs of the duplex DNA with a gap of 1 intercalation site between EG binding sites, as expected for a bifunctional molecule. Interestingly, at high [EG]/[base pair], the intercalation is disrupted. A model is proposed based on the fluorescence spectrum where the formation of anti-parallel stacked chains of EGs bound externally to the duplex DNA occur at these high ratios.

**ABBREVIATIONS**

AO-acridine orange, DNA-deoxyribonucleic acid, EDTA-ethylenediamminetetraacetic acid, EG-EvaGreen, RNA-ribonucleic acid, RT-PCR-reverse transcription polymerase chain reaction.

## INTRODUCTION

Noncovalent binding of small molecules with DNA is of fundamental importance in biology because DNA plays a key role in basic life processes such as metabolism, regulation, and immunity[1–4]. Intercalation of small molecules to DNA can disrupt replication and/or transcription leading to cancer and cell death[5,6]. The study of small molecule interactions with DNA has a key role in pharmacology, because DNA can be a target for anticancer and antibiotic drugs[7–12].

EvaGreen (EG) is a DNA intercalating dye[13–17]. EG intercalation into dsDNA is not sequence specific[18] and it has a weak affinity for binding to single-stranded DNA. It is weakly fluorescent in aqueous solution, but becomes highly fluorescent when it intercalates in double-stranded DNA (dsDNA). The dye is thermally and hydrolytically stable[18]. It is also nonmutagenic and noncytotoxic, because it is impermeable to cell membranes[19]. These properties provide EvaGreen with many advantages over other commonly used dyes, such as SYBR Green I, in applications ranging from quantitative RT-PCR, high resolution DNA melt curve analysis, routine DNA quantification, and capillary gel electrophoresis[13-18]. Despite its increasing applications in biology, the binding interactions of EG with DNA have not yet been quantified.

The biological activity of intercalating ligands arises partly due to the fact that intercalation unwinds the helix and lengthens the DNA to accommodate the ligand and these conformational modifications can lead to inhibition of transcription, replication and DNA repair processes thereby making intercalators potent carcinogens[5-12,20–25]. On the other hand, these properties make intercalators, including acridine orange (AO), attractive candidates for the development of DNA targeted drugs and chemotherapy[5-12,20-25]. In addition, intercalating dyes are used for staining and routine quantification of DNA[13,14,17,18,26].

EvaGreen is composed of two AO moieties connected by a flexible N,N'-(oxydi-2,1-ethanediyl)bis-decanamide linker containing 20 single bonds, shown in Scheme 1. In aqueous solution, the hydrophobic planar fused aromatic rings form a weakly fluorescent dimer[18] of stacked AO chromophores, described here as the "closed form". The dimer dissociates upon bis-intercalation of the planar AO moieties between the base pairs of dsDNA, giving rise to two highly fluorescent monomeric AOs still connected by the linker, described here as the “open form”[27–31].

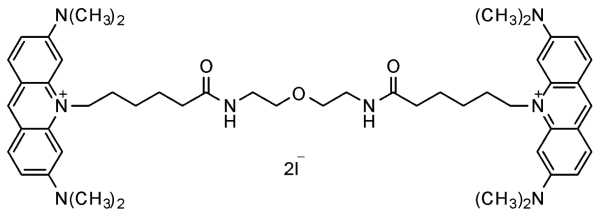


Open form

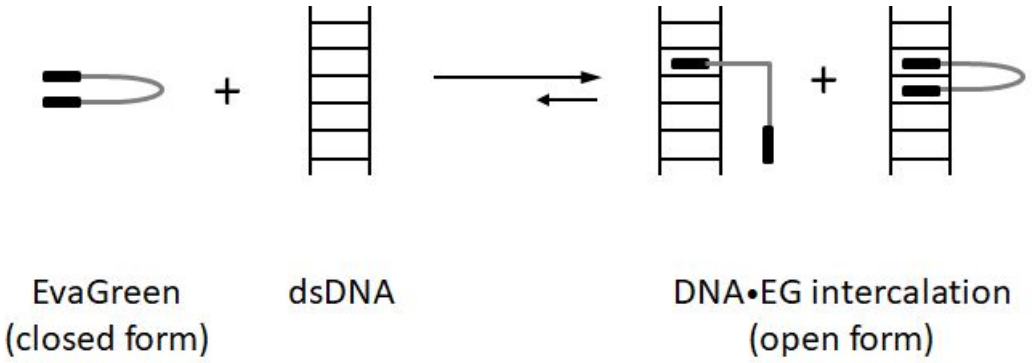


Scheme 1. Molecular structure of EvaGreen (EG, top) and a schematic of the EG intercalation into dsDNA (bottom). The EvaGreen dye consists of two AO moieties covalently bonded to the ends of an N,N'-(oxydi-2,1-ethanediyl)bis-decanamide linker. EG in dilute aqueous solutions is weakly fluorescent in the native dimer form ("closed form") but is highly fluorescent in the "open form" when it intercalates into dsDNA.

The most commonly used method for quantification of DNA is to determine the UV absorbance at 260 nm. Absorbance at 260 nm is also commonly used for the determination of the dsDNA melting temperature by taking advantage of the loss of hypochromicity accompanying the dissociation of the DNA duplex[32]. However, absorbance measurements alone cannot differentiate single-stranded from double-stranded DNA, since the absorption in this region originates from the nucleobases in the DNA. Furthermore, many other biomolecules, including proteins, ions, and other impurities present in the solution, may interfere and thereby limit the applications of absorption techniques for DNA quantification.

Fluorescence detection is a simple and highly sensitive method for quantification of DNA. Because fluorescent dyes used for labeling can bind selectively to dsDNA via intercalation, the

minor groove, or the major groove, fluorescence detection can be used for routine DNA quantification and real-time quantitative PCR with minimal interference. In the last few years, fluorescence techniques based on molecular beacons, smart probes, rare earth cations, and other fluorescence probes have been developed for the quantification and characterization of UV-induced damage to DNA[33–46] In this paper, we measure and characterize EvaGreen, a next-generation green fluorescent nucleic acid dye, and its binding interactions with DNA by using the Scatchard, and McGhee and von Hippel models.

## EXPERIMENTAL

### Materials

EvaGreen (EG) in aqueous solution with certified 25 μM dye content was purchased from Biotium (Hayward, CA) and stored at -20 °C. Sodium chloride, *tris*(hydroxymethyl)aminomethane (Tris), and ethylenediamminetetraacetic acid (EDTA) disodium salt were obtained from EMD Chemicals Inc. (Gibbstown, New Jersey), ICN Biomedicals (Aurora, Ohio) and BDH Inc. (Toronto, Ontario), respectively. All chemicals were used as received. Nanopure water from a Barnsted Nanopure (Boston, Massachusetts) system was used for all solution preparation. Single-stranded $dA_{17}$ and $dT_{17}$ deoxyribooligonucleotide targets purified by standard desalting were obtained from Integrated DNA Technologies Inc. (Coralville, Iowa). The oligonucleotide samples were centrifuged and dissolved in the desired volumes of nanopure water to obtain 581.8 μM oligonucleotide solutions and stored at −20 °C until needed.

**Instrumentation**

Absorption and fluorescence spectra of sample solutions were recorded using a Hewlett-Packard (Sunnyvale, California) 8452A diode array spectrophotometer and a Photon Technologies International (Birmingham, New Jersey) fluorescence spectrophotometer, respectively. A SpectraMax i3x Multi-Mode microplate reader controlled by SoftMax from Molecular Devices, LLC (Sunnyvale, California) was used to record the fluorescence spectra. Sample solutions for the microplate reader were prepared in a clear-bottom 96-well plate from Corning (Corning, New York).

**Preparation of duplex poly-$dA_{17}$·poly-$dT_{17}$**

Equal volumes of the 581.8 μM complementary oligos were mixed in an Eppendorf tube and diluted to give a final concentration of 131 μM duplex DNA (6.6 mM Tris, 0.6 mM EDTA, 3.5 mM NaCl, pH 7.5). The solution was heated in a water bath while stirring at the annealing temperature of 95 °C for about 5 min and then allowed to equilibrate to room temperature. The annealed duplex poly-$dA_{17}$·poly-$dT_{17}$ solution was stored at -20 °C until needed.

**Analysis**

The solution for analysis typically contained ~0.2 μM dsDNA (10 mM Tris buffer, 1 mM EDTA, 10 mM NaCl, pH 7.5) to which was added EG to a final concentration of 0.67 μM. After the addition of EG, the solutions were incubated at 37-42 °C for 20 min and allowed to equilibrate for >1 hr to room temperature. The fluorescence spectra of 200 μL/well solutions in a

96-well plate were recorded with 470 nm excitation. The emitted fluorescence intensity was measured at 532 nm. The software for nonlinear least-squares analysis was Microcal Origin (Microcal Origin, Northampton, MA).

## RESULTS AND DISCUSSION

The noncovalent binding interactions between DNA and one or more ligands play a key role in the effect small molecules can have on biological functions such as molecular recognition, DNA replication, and DNA transcription. Ligands can bind to DNA noncovalently in three different ways, intercalation, minor or major groove binding, or electrostatically. Noncovalent binding interactions due to intercalation, of concern here for EG, involve reversible insertion between the stacked base pairs of dsDNA of a molecule typically composed of one or more planar fused aromatic rings. Figure 1 shows the absorption and fluorescence spectra of a mixture of EG and dsDNA•EG bound complex.

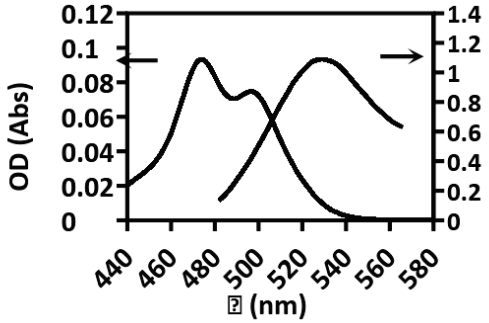


Figure 1. Absorption and fluorescence spectra of a solution containing 0.2 μM poly-$dA_{17}$·poly-$dT_{17}$ dsDNA and 2.5 μM EG in buffered (10 mM Tris, 1 mM EDTA, 10 mM

NaCl, pH 7.5) aqueous solution. The fluorescence spectrum was recorded with 470 nm excitation.

The spectra of EG in the presence of dsDNA in Figure 1 have maxima at 474 and 490 nm for absorption and at 532 nm for fluorescence, and are similar to those reported in the literature[18]. EG in the absence of duplex DNA has a weak fluorescence, typically more than an order of magnitude less than bound EG. The fluorescence intensity increases upon binding of EG to duplex DNA and the spectrum shifts bathochromically to longer wavelengths.

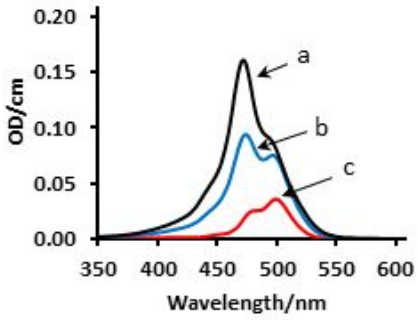


Figure 2. Absorption spectra of (a) 2.5 μM EG, (b) 2.5 μM EG in the presence of 0.2 μM duplex DNA in buffer solutions (10 mM NaCl, 1 mM EDTA, 10 mM Tris, pH 7.5), and (c) dsDNA•EG complex obtained by spectral subtraction i.e. spectrum c = spectrum b – (0.4663 X spectrum a).

The spectrum of pure dsDNA•EG complex formed at any particular EG concentration was obtained by subtracting the spectrum of EG in solution without dsDNA (free EG) from that of the spectrum of EG solution containing 0.2 μM dsDNA with both solutions containing similar concentration of EG (Figure 2). In the spectral subtraction, the spectral intensity of the EG solution containing 0.2 μM dsDNA was kept constant while adjusting the spectral intensity of

the free EG until (1) the background in the 550-600 nm region showed no negative absorbance features, and (2) the previously published[47] spectrum of dsDNA•EG complex was obtained. Due to the strong overlap in the absorption spectra of free EG and the dsDNA•EG complex in the 400-480 nm region, this spectra subtraction does carry with it large error bars (Figure 3). It is however important to note that the spectrum of the dsDNA•EG complex reported here is very similar to that reported in the literature[47].

To quantitatively measure the nature of the binding interaction, the concentrations of the free and bound EG need to be determined. The equilibrium concentration of free EG in the presence of DNA ($[EG]_{eq}$) was determined from the difference in the absorption spectra of EG in the presence and absence of 0.2 μM duplex DNA. This is possible because EG in solution has an absorption spectrum distinct from that of the intercalated EG, the latter of which exhibits an absorption spectrum similar to monomeric AO[27-31,48,49]. The formation of dimers and higher aggregates of AO in aqueous solution has been extensively studied[29,49,50-53]. The absorption spectra of different EG concentrations in the absence and presence of duplex DNA in solution are shown in Figure 3.

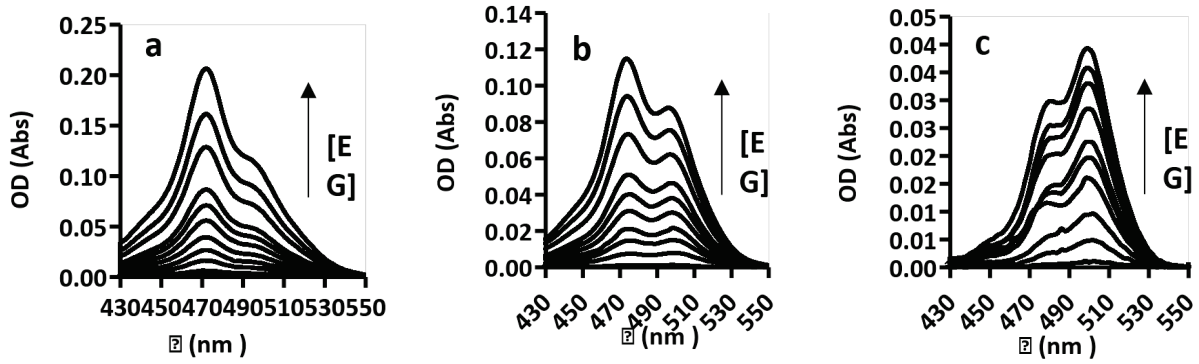


Figure 3. Absorption spectra recorded in the (a) absence and (b) presence of 0.2 μM duplex DNA in solutions containing different [EG] (0.1, 0.2, 0.4, 0.6, 0.8, 1.0, 1.2, 1.5, 2.0, 2.5, & 3.0 μM) in buffer (10 mM NaCl, 1 mM EDTA, 10 mM Tris, pH 7.5). (c) The difference spectra corresponding to the DNA•EG complex are obtained by spectral subtraction (using GRAMS software) of the spectra (b – a) at each [EG]. To obtain the spectrum of the pure DNA•EG complex (c) at a particular [EG], the intensity of the EG spectrum (a) is adjusted and subtracted from the spectrum in (b) until no absorbance is observed in the 600-650 nm region.

The absorption spectrum of EG in the free state has a peak at 472 nm (Figure 3a) similar to the previously reported spectrum of AO dimers[54]. However, the spectrum of the intercalated EG (Figure 3c) is similar to the previously reported spectrum of AO monomers[48-53]. This indicates that the intercalation of the AO moieties of EG between the base pairs of dsDNA does not lead to significant alteration of the electronic structure of the monomeric AO moiety, but is sufficient to disrupt any interaction between the two electronic structures of the AO monomers in each EG molecule. The absorption spectrum of EG intercalated or bound to dsDNA, dsDNA•EG complex, has a maximum at ~500 nm (Figure 3c), and the optical density at 500 nm ($OD_{500}$) was

used to obtain the concentration of bound EG, $[EG]_b=OD_{500}/\varepsilon_{500}$. The molar absorption coefficient ($\varepsilon_{500}$) of the dsDNA•EG complex obtained from $OD_{500}$ and $[EG]_b$ (where $[EG]_b = [EG]_t - [EG]_{eq}$, and $[EG]_t$ and $[EG]_{eq}$ are the total and free EG concentrations, respectively). is similar to those reported for monomeric AO in the literature[48-53].

The free EG concentration in the presence of dsDNA, $[EG]_{eq}$, can be calculated from the absorption spectrum of the pure dsDNA•EG complex (Figure 3c, $[EG]_b$) and the spectrum containing both free EG in solution and the dsDNA•EG complex (Figure 2b, $[EG]_{eq}+ [EG]_b$). From the Beer-Lambert law, $[EG]_{eq} = \Delta OD_{472}/\varepsilon_{472}$, where $\varepsilon_{472}$ is the absorption coefficient of EG (70,200 $M^{-1}$ $cm^{-1}$), and $\Delta OD_{472}$ is the difference in absorbance at 472 nm between the spectrum of the solution containing both EG and dsDNA (Figure 3b) and that of the dsDNA•EG complex (Figure 3c) at each EG concentration. The free EG concentration will be important in quantifying the nature of the binding between EG and dsDNA.

In order to gain insight into the binding interaction between the duplex DNA (poly-$dA_{17}$·poly-$dT_{17}$) and EG, the binding isotherm in the traditional graphical representation is plotted as shown in Figure 4.

.

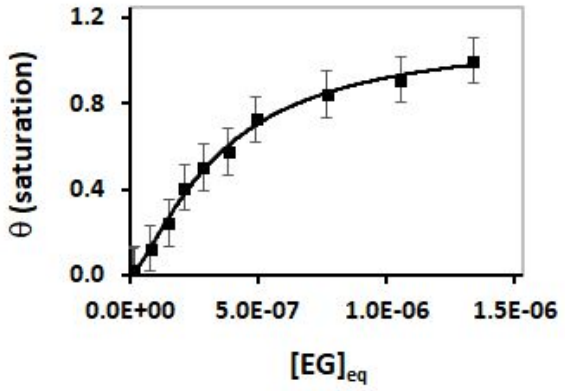


Figure 4. Binding isotherm for the intercalation of EG into 0.2 μM duplex poly-$dA_{17}$·poly-$dT_{17}$ (10 mM Tris, 1 mM EDTA, 10 mM NaCl, pH 7.5). The data points represent the average and standard deviation (error bars) from 4 separate experiments. The curve is the fit to the experimental data with the Hill equation (see supplementary information) using the parameters $K_a^m$ = (2.9±0.3) x$10^6$ and m = 1.4±0.1.

The fractional saturation binding (θ) of EG to a dsDNA (Figure 3) was calculated by normalizing the binding density, $[EG]_b/[DNA]_{total}$, the number of bound EG per dsDNA oligomer obtained from the ratio of concentration of bound EG ($[EG]_b$) to the total concentration of (0.2 μM) duplex DNA ($[DNA]_{total}$).

The relationship between fractional saturation (θ), the equilibrium constant, and the degree of cooperativity describing the interaction of a protein and a dsDNA was first derived by Hill[55] (see supplementary information). In Figure 4, the Hill model fit to the isotherm of EG binding to dsDNA is displayed to show that it can provide information about the nature of the interaction. However, it is important to note that the Hill equation cannot be used for the analysis of most of

the ligand-receptor binding interactions except for the cases describing either a simple 1:1 noncooperative binding or a binding interaction which induces extreme positive cooperativity in the receptor for the binding of the subsequent ligands.

The most widely-used approach for analyzing the problem of nonspecific binding of ligands to one-dimensional lattices, such as the isotherm for ligand binding to dsDNA, is the neighbor exclusion model based on conditional probability approach developed by McGhee and von Hippel[56].

$$\frac{r}{[EG]_{eq}} = K_a (1 - nr) \left[ \frac{(2\omega-1)(1-nr)+r-R}{2(\omega-1)(1-nr)} \right]^{n-1} \left[ \frac{1-(n+1)r+R}{2(1-nr)} \right]^2 \qquad (2)$$

Where, $K_a$ is the intrinsic affinity constant for binding one EG to dsDNA which has no bound ligand, ω is the cooperativity parameter, n is the occluded site size (the number of overlapping base pairs effectively occupied by a bound ligand), $r = [EG]_b/[bp]_{total}$ is the number of bound ligands per lattice site calculated from absorption spectra (Figure 2) and $[bp]_{total}$ = 17 x $[dsDNA]_{total}$ for duplex poly-$dA_{17}$·poly-$dT_{17}$, $R = \left\{ [1-(n+1)r]^2 + 4\omega r(1-nr) \right\}^{1/2}$. The cooperativity parameter ω is equal to the equilibrium constant for moving a ligand from an isolated site to a singly contiguous one or from a singly contiguous site to a doubly-contiguous one.

The model assumes that the DNA lattice consists of a one-dimensional array of identical and noninteracting potential binding sites of infinite length represented by the number of base

pairs in duplex DNA. A ligand binding to any site occludes the neighboring sites from binding as defined by the site size parameter, n. Since many systems of interest deal with DNA oligomers of finite length, Epstein[57] adopted a combinatorial approach to calculate an exact expression for the extent of ligand binding to a one-dimensional lattice of finite length. However, this model for the finite lattice isotherm does not simplify to a closed-form expression and its implementation is convoluted, as it involves factorial-based terms to explicitly enumerate all the possible states of bound ligands in the lattice. In addition, Epstein[57] demonstrated that the McGhee and von Hippel infinite lattice equation provides a good approximation for the binding isotherm even for short lattices. Recently, Tsodikov, et al.[58] using the analytical McGhee and von Hippel infinite-lattice nonspecific binding isotherm derived an analytic expression for nonspecific binding of ligands to a finite lattice by incorporating end effects. Within this model, the closed analytical form of the McGhee and von Hippel equation in the Scatchard[59] representation has the form[60,61].

$$\frac{r}{[EG]_{eq}} = K_a(1-nr)\left[\frac{(2\omega-1)(1-nr)+r-R}{2(\omega-1)(1-nr)}\right]^{n-1}\left[\frac{1-(n+1)r+R}{2(1-nr)}\right]^{2}\left[\frac{N-n+1}{N}\right] \qquad (3)$$

Where, N is the length of the DNA in base pairs, and the factor (N-n+1)/N accounts for the end effects on nonspecific binding to a finite lattice. In order to obtained the binding parameter for the interaction of EG with duplex poly-$dA_{17}$·poly-$dT_{17}$, the experimentally-determined isotherm for the nonspecific binding of EG into duplex DNA is presented in the form of Scatchard plot as shown in Figure 5.

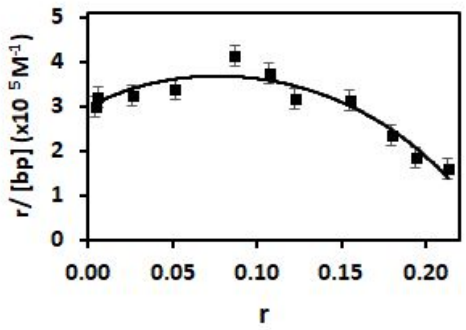


Figure 5. Scatchard plot of the binding isotherm for nonspecific intercalation of EG into duplex poly-$dA_{17}$·poly-$dT_{17}$. The curve is the fit to the experimental data (square points) using Equation 3 with $K_a$= (3.6±0.2) x$10^5$ $M^{-1}$, n = 4.0±0.1 and ω = 8.1±1.0. The data points represent the average (square points) and standard deviation (error bars) from 4 separate experiments.

The experimental binding data was fit with Equation 3 using nonlinear least-squares analysis with (3.6±0.2) x$10^5$ $M^{-1}$, n = 4.0±0.1 and ω = 8.1±1.0 characterizing the binding interactions between EG and duplex poly-$dA_{17}$·poly-$dT_{17}$. The observed affinity constant ($K_a$) is in the range expected[62,63] for similar ligand intercalation into duplex poly-$dA_{17}$·poly-$dT_{17}$, and the cooperativity parameter value (ω) of 8.1 is similar to the value reported for bifunctional diacridines[64-66]. The occluded site size of n = 4 indicates that the intercalating EG molecule (two AO moieties linked by 20 flexible single bonds) occupies or blocks off 4 consecutive base pairs in the poly-$dA_{17}$·poly-$dT_{17}$ duplex as shown in Scheme 2.

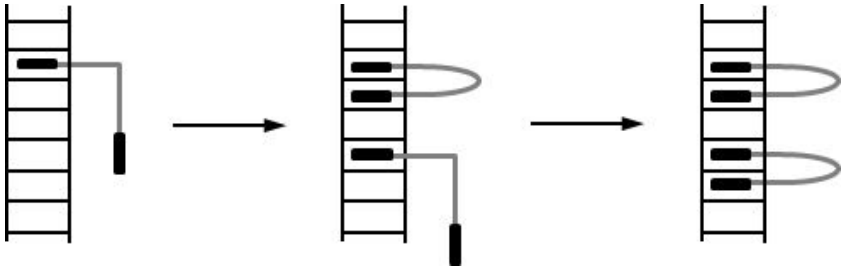

Scheme 2. Depiction of a possible route to a sequential binding of bisintercalators (two AO moieties linked by 20 flexible single bonds) to a dsDNA with occluded site size of n = 4. The binding of bifunctional EG into dsDNA violates the neighbor-exclusion principle (i.e. n < 5 for a two-site intercalator).

An alternative binding scheme which follows the normal neighbor-exclusion principle for bisintercalators would require n = 5. Clearly, for a bifunctional EG molecule, the binding of the first AO into dsDNA may facilitate the binding of the second AO to the adjacent site in the dsDNA, presumable due to the proximity of the two moieties as they are linked by 20 flexible single bonds. Thus, the proximity effect could overcome the barrier to binding into the adjacent site resulting from structural changes such as unwinding, lengthening, and reduction of electrostatic interactions (anionic phosphate groups) in dsDNA induced by binding of the first AO group.

It is important to note that different nucleotide sequences show distinct propensities to deform, bend, and twist on their own or upon binding to dye, protein, and drug targets.[67-72] For instance, the pyrimidine-purine doublets, e.g. TA, CG, etc., are the most conformationally flexible doublets, and the purine-purine doublets, e.g. AA and GG, are the most conformationally rigid doublets. Thus, the structural rigidity of A-tracts for the duplex poly-$dA_{17}$•poly-$dT_{17}$ with

long persistence lengths could have a strong influence on the binding parameters. However, EG is known to bind essentially sequence independent[18].

The binding interaction of AO with duplex DNA has been extensively investigated[23,28-31,62-66], and these studies have shown that there are at least three kinds of species present in the binding of AO to duplex DNA, strong binding or intercalation in which the dye molecule inserts between two neighboring base pairs, half-intercalated dimeric molecules in which the protruding portion of the partially intercalated AO molecules is coupled to another AO molecule, and dimeric dye molecules that bind electrostatically with the anionic phosphate groups and form anti-parallel stacked chains[30,73,74] These three types of DNA•AO complexes are observed at low, intermediate, and high dye/DNA concentration ratios, respectively. In order to study the formation of similar species in the binding of EG to duplex poly-$dA_{17}$·poly-$dT_{17}$, the EG fluorescence intensity in the presence of duplex poly-$dA_{17}$·poly-$dT_{17}$ was measured at higher dye concentrations. The results are shown in Figure 6.

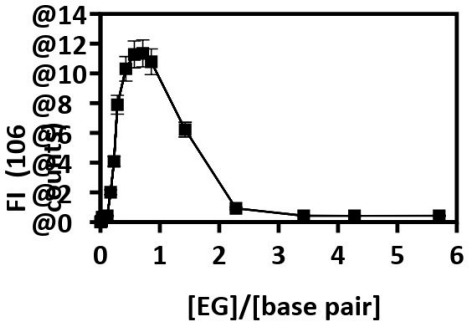

Figure 6. The fluorescence intensity (FI) at 532 nm (excitation 470 nm) as a function of the [EG]/[bp] ratio. The base-pair concentration was held constant at 3.5 μM and the EG concentration was varied in the 0.01-20 μM range. The line drawn is to guide the eye.

As seen in Figure 6 for low dye concentrations, the fluorescence intensity increases with increasing [EG]/[bp] ratio, plateauing at [EG]/[bp]≈0.7. The fluorescence intensity then decreases above this [EG]/[bp] ratio, presumably due to the increase in the number of half-intercalated dimeric molecules and/or stacked anti-parallel chains, as discussed above. At [EG]/[bp]>2, the fluorescence intensity has decreased to a value comparable to that of free EG in solution without DNA.

To interpret the fate of the intercalated EG, fluorescence spectra of EG at these high concentrations in the presence of duplex poly-$dA_{17}$·poly-$dT_{17}$ were obtained. The results are shown in Figure 7a. In duplex DNA solutions with low [EG]/[bp] ratios, the fluorescence spectra have maxima at 532 nm, virtually unaffected by an increase in [EG]/[bp] ratios up to about 1.4. As the [EG]/[bp] ratio is increased above 1.4, the fluorescence spectrum is redshifted, with the wavelength maximum of 532 nm shifting to 630 nm (Figure 7a). This indicates formation of a new species similar to the fluorescence from the association of AO with RNA[75,76].

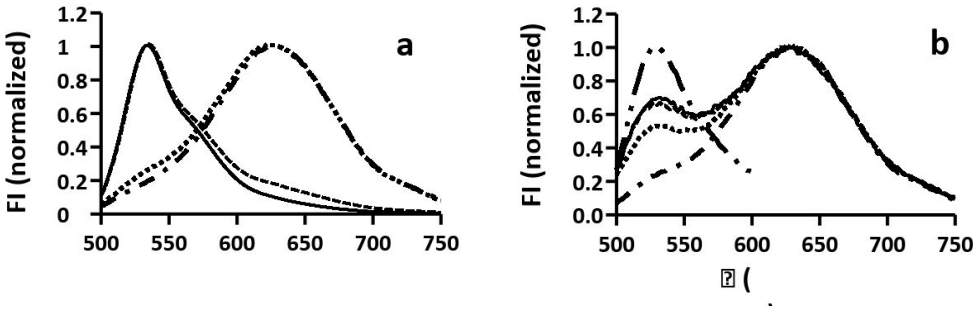


Figure 7. Normalized fluorescence spectra of (a) DNA•EG intercalated complexes and of (b) EG in the absence of dsDNA in buffered aqueous solutions. The concentrations of EG in both (a) and (b) are 2.5 (solid line), 5 (dashed line), 8 (dotted line), and 20 μM (dot-dashed line) corresponding to [EG]/[bp] ratios of 0.7, 1.4, 2.3 and 5.7, respectively. The solutions in (a) also contain 0.2 μM dsDNA. The dot-dot-dashed line in (b) is the normalized fluorescence spectrum of 0.7 μM free EG in solution.

In order to gain insight into the species formed at the higher [EG]/[bp] ratio, the fluorescence spectra of EG alone, i.e. in the absence of dsDNA, were also recorded as shown in Figure 7b. The fluorescence spectra of EG in the absence of dsDNA shows a shift of the 530 nm peak to a 630 nm peak with increasing EG concentration. In fact, the fluorescence spectra recorded from solutions containing 20 μM EG with and without 0.2 μM dsDNA are virtually identical (Figure 7), indicating that they have similar composition and structure. In other words, at [EG]/[bp]>2 the intercalation of EG with dsDNA is disrupted by the likely formation of anti-parallel stacked EG chains electrostatically attached to the dsDNA. Since intercalation is a dynamic process with weak binding interaction energy (7.6 kcal/mol) and given the fact that EG has the tendency to form dimer and higher aggregates, it is reasonable to model the EG structure as anti-parallel

stacked chains over intercalated EG-dsDNA at high [EG]/[bp] ratio. This model of EG anti-parallel stacked chains at high [EG]/[bp] ratios requires further characterization.

## CONCLUSIONS

EvaGreen (EG) intercalates cooperatively into the base pairs of duplex DNA with an intrinsic affinity constant of 3.6 X $10^5$ $M^{-1}$ and an occluded site size of 4 indicating that two AO moieties in the EG dye intercalate into the adjacent base pairs of the dsDNA in contravention to the well-known neighbor exclusion principle which is a rule normally followed by mono-functional molecules. As EG dye predominantly exists as a dimer in dilute solutions and the AO moieties that make up EG have a tendency to form aggregates at high concentrations, it is plausible to imagine that the anti-parallel stacked chains of EG dyes dominate over intercalated EG-dsDNA in solutions containing a high concentration of EG. The formation of anti-parallel stacked chains of EGs bound externally to the dsDNA could be facilitated by electrostatic interactions between the dye and the phosphate backbone of the duplex. These findings can have strong implications in the applications of EG dye in quantitative RT-PCR, high resolution DNA melt curve analysis, routine DNA quantification, and capillary gel electrophoresis.

### Conflict of Interest

The Authors declare that there are no conflicts of interest associated with the manuscript.

**References**


1. Riley, K. E. & Hobza, P. Noncovalent interactions in biochemistry. *Wiley Interdiscip. Rev. Comput. Mol. Sci.* **1,** 3–17 (2011).
2. Strekowski, L. & Wilson, B. Noncovalent interactions with DNA: an overview. *Mutat. Res.* **623,** 3–13 (2007).
3. McCammon, J. A. Theory of biomolecular recognition. *Curr. Opin. Struct. Biol.* **8,** 245–249 (1998).
4. Du, Y. H., Huang, J., Weng, X. C. & Zhou, X. Specific Recognition of DNA by Small Molecules. *Curr. Med. Chem.* **17,** 173–189 (2010).
5. Biebricher, A. S. *et al.* The impact of DNA intercalators on DNA and DNA-processing enzymes elucidated through force-dependent binding kinetics. *Nat. Commun.* **6,** 7304 (2015).
6. Lenglet, G. & David-Cordonnier, M.-H. DNA-Destabilizing Agents as an Alternative Approach for Targeting DNA: Mechanisms of Action and Cellular Consequences. *J. Nucleic Acids* **2010,** 1–17 (2010).
7. Neidle, S. & Thurston, D. E. Chemical approaches to the discovery and development of cancer therapies. *Nat. Rev. Cancer* **5,** 285–96 (2005).
8. Belizário, J. E., Sangiuliano, B. A., Perez-Sosa, M., Neyra, J. M. & Moreira, D. F. Using pharmacogenomic databases for discovering patient-target genes and small molecule candidates to cancer therapy. *Front. Pharmacol.* **7,** 1–16 (2016).
9. Persil, Ö. & Hud, N. V. Harnessing DNA intercalation. *Trends Biotechnol.* **25,** 433–436 (2007).

10. Rescifina, A., Zagni, C., Varrica, M. G., Pistarà, V. & Corsaro, A. Recent advances in small organic molecules as DNA intercalating agents: Synthesis, activity, and modeling. *Eur. J. Med. Chem.* **74,** 95–115 (2014).

11. Palchaudhuri, R. & Hergenrother, P. J. DNA as a target for anticancer compounds: methods to determine the mode of binding and the mechanism of action. *Curr. Opin. Biotechnol.* **18,** 497–503 (2007).

12. Martínez, R. & Chacón-García, L. The search of DNA-intercalators as antitumoral drugs: what it worked and what did not work. *Curr. Med. Chem.* **12,** 127–151 (2005).

13. Wang, W., Chen, K. & Xu, C. DNA quantification using EvaGreen and a real-time PCR instrument. *Anal. Biochem.* **356,** 303–305 (2006).

14. Eischeid, A. C. SYTO dyes and EvaGreen outperform SYBR Green in real-time PCR. *BMC Res. Notes* **4,** 263 (2011).

15. Radvanszky, J., Surovy, M., Nagyova, E., Minarik, G. & Kadasi, L. Comparison of different DNA binding fluorescent dyes for applications of high-resolution melting analysis. *Clin. Biochem.* **48,** 609–616 (2015).

16. González-Giraldo, Y., Rodríguez-Dueñas, M. & Forero, D. A. Development of Novel High-Resolution Melting-Based Assays for Genotyping Two Alu Insertion Polymorphisms (FXIIIB and PV92). *Mol. Biotechnol.* **58,** 197–201 (2016).

17. Ihrig, J., Lill, R. & Mühlenhoff, U. Application of the DNA-specific dye EvaGreen for the routine quantification of DNA in microplates. *Anal. Biochem.* **359,** 265–267 (2006).

18. Mao, F., Leung, W.-Y. & Xin, X. Characterization of EvaGreen and the implication of its physicochemical properties for qPCR applications. *BMC Biotechnol.* **7,** 76 (2007).

19. https://biotium.com/wp-content/uploads/2013/07/EG-safety.pdf. Safety Report of EvaGreen ® Dye. 10 (2011).

20. Demeunynck, M. Antitumour acridines. *Expert Opin. Ther. Pat.* **14,** 55–70 (2004).

21. Denny, W. Acridine derivatives as chemotherapeutic agents. *Curr Med Chem.* **9,** 1655–1665 (2002).

22. Galdino-Pitta M. R., Pitta M.G. R., Lima M.C. A., Galdino S. L., P. I. R. Niche for Acridine Derivatives in Anticancer Therapy. *Mini-Reviews Med. Chem.* **13,** 1256–1271 (2013).

23. Georghiou, S. Interaction of Acridine Drugs With Dna and Nucleotides. *Photochem. Photobiol.* **26,** 59–68 (1977).

24. Martine Demeunynck, B. S. P., Franck Charmantray, B. S. P. & Alain Martelli, B. S. P. Interest of Acridine Derivatives in the Anticancer Chemotherapy. *Curr. Pharm. Des.* **7,** 1703–1724 (2001).

25. Matsubara, T. *et al.* Acridine orange used for photodynamic therapy accumulates in malignant musculoskeletal tumors depending on pH gradient. *Anticancer Res.* **26,** 187–193 (2006).

26. Bruijns, B. B., Tiggelaar, R. M. & Gardeniers, J. G. E. Fluorescent cyanine dyes for the quantification of low amounts of dsDNA. *Anal. Biochem.* **511,** 74–79 (2016).

27. Lǒber, G. The fluorescence of dye-nucleic acid complexes. *J. Lumin.* **22,** 221–265 (1981).

28. Kubota, Y. & Steiner, R. F. Fluorescence decay and quantum yield characteristics of acridine orange and proflavine bound to DNA. *Biophys. Chem.* **6,** 279–289 (1977).

29. Sayed, M., Krishnamurthy, B. & Pal, H. Unraveling multiple binding modes of acridine

orange to DNA using a multispectroscopic approach. *Phys. Chem. Chem. Phys.* **18,** 24642–24653 (2016).

30. Fredericq, E. & Houssier, C. Study of the interaction of DNA and acridine orange by various optical methods. *Biopolymers* **11,** 2281–2308 (1972).

31. Fornaslero, D. Circular Dichroism Spectra and the Interaction between Acridine Dyes and Deoxyribonucleic Acid. *J. Phys. Chem.* **85,** 613–618 (1981).

32. DNA Duplex Stability. http://www.atdbio.com/content/53/DNA-duplex-stability. *DNA Duplex Stability*

33. El-Yazbi, A. F. & Loppnow, G. R. Detecting UV-induced nucleic-acid damage. *TrAC - Trends Anal. Chem.* **61,** 83–91 (2014).

34. Nair, S. G. & Loppnow, G. R. Multiplexed, UVC-induced, sequence-dependent DNA damage detection. *Photochem. Photobiol.* **89,** 884–890 (2013).

35. Yarasi, S., McConachie, C. & Loppnow, G. R. Molecular beacon probes of photodamage in thymine and uracil oligonucleotides. *Photochem. Photobiol.* **81,** 467–73 (2005).

36. Leslie, D. C. *et al.* New detection modality for label-free quantification of DNA in biological samples via superparamagnetic bead aggregation. *J. Am. Chem. Soc.* **134,** 5689–5696 (2012).

37. Haque, K. a *et al.* Performance of high-throughput DNA quantification methods. *BMC Biotechnol.* **3,** 20 (1-10) (2003).

38. Olive, P. L. & Banáth, J. P. The comet assay: a method to measure DNA damage in individual cells. *Nat. Protoc.* **1,** 23–29 (2006).

39. Wilhelm, J. & Pingoud, A. Real-Time Polymerase Chain Reaction. *ChemBioChem* **4,**

1120–1128 (2003).

40. Ludwig Brand and James R. Gohlke. Fluorescence Probes for Structure. *Annu. Rev. Biochem.* **41,** 843–868 (1972).

41. Morozkin, E. S., Laktionov, P. P., Rykova, E. Y. & Vlassov, V. V. Fluorometric quantification of RNA and DNA in solutions containing both nucleic acids. *Anal. Biochem.* **322,** 48–50 (2003).

42. Kong, J. J., Chen, Z. P., Chen, Y., Yan, X. F. & Yu, R. Q. Direct DNA quantification in cell lysates by fluorometric method in combination with an advanced chemometric model. *Chemom. Intell. Lab. Syst.* **151,** 9–14 (2016).

43. Le Pecq, J.-B. & Paoletti, C. A new fluorometric method for RNA and DNA determination. *Anal. Biochem.* **17,** 100–107 (1966).

44. Nielsen, K. *et al.* Comparison of five DNA quantification methods. *Forensic Sci. Int. Genet.* **2,** 226–230 (2008).

45. Shokere, L. A., Holden, M. J. & Ronald Jenkins, G. Comparison of fluorometric and spectrophotometric DNA quantification for real-time quantitative PCR of degraded DNA. *Food Control* **20,** 391–401 (2009).

46. Dhawan, A., Bajpayee, M. & Parmar, D. Comet assay: A reliable tool for the assessment of DNA damage in different models. *Cell Biol. Toxicol.* **25,** 5–32 (2009).

47. Amado, A.M., Pazin, W. M., Ito, A. S., Kuzmin, V. A., Borissevitch, I. E. Acridine orange interaction with DNA: Effect of ionic strength. *Biochim. Biophys. Acta Gen. Subj* **1861,** 900-909 (2017).

48. Dsouza, R. N., Pischel, U. & Nau, W. M. Fluorescent Dyes and Their Supramolecular

Host / Guest Complexes with Macrocycles in Aqueous Solution. *Chem. Rev.* **111,** 7941–7980 (2011).

49. Shaikh, M., Mohanty, J., Singh, P. K., Nau, W. M. & Pal, H. Complexation of acridine orange by cucurbit[7]uril and beta-cyclodextrin: photophysical effects and pKa shifts. *Photochem. Photobiol. Sci.* **7,** 408–414 (2008).

50. Lucla Costantlno, G. *et al.* Acridine Orange Association Equilibrium. *J. Chem. Eng. data* **29,** 62–66 (1984).

51. Luchowski, R. & Krawczyk, S. Stark effect spectroscopy of exciton states in the dimer of acridine orange. *Chem. Phys.* **293,** 155–166 (2003).

52. B. H. Robinson, A. L. and G. S. Thermodynamic behaviour of acridine orange in solution. Model system for studying stacking and charge-effects on self-aggregation. *J. Chem. Soc. Faraday Trans. I* **69,** 56–69 (1973).

53. Lamm, M. E. & Neville, D. M. The Dimer Spectrum of Acridine Orange Hydrochloride. *J. Phys. Chem.* **69,** 3872–3877 (1965).

54. Dragan, A. I. *et al.* Characterization of PicoGreen interaction with dsDNA and the origin of its fluorescence enhancement upon binding. *Biophys. J.* **99,** 3010–3019 (2010).

55. Hill, A. V. The possible effects of the aggregation of the molecules of haemoglobin on its dissociation curves. *J. Physiol.* **40,** iv–vii (1910).

56. McGhee, J. D. & Hippel, P. H. V. Theoretical Aspects of DNA-Protein Interactions - Cooperative and Non-Cooperative Binding of Large Ligands to A One-Dimensional Homogeneous Lattice. *J. Mol. Biol.* **86,** 469–489 (1974).

57. Epstein, R. I. polynucleotide and the Iigand. *Biophys. Chem.* **8,** 327–339 (1978).

58. Tsodikov, O. V, Holbrook, J. a, Shkel, I. a & Record, M. T. Analytic binding isotherms describing competitive interactions of a protein ligand with specific and nonspecific sites on the same DNA oligomer. *Biophys. J.* **81,** 1960–9 (2001).

59. Scatchard, G. the Attractions of Proteins for Small Molecules and Ions. *Ann. N. Y. Acad. Sci.* **51,** 660–672 (1949).

60. Melikishvili, M. & Fried, M. G. Resolving the contributions of two cooperative mechanisms to the DNA Binding of AGT. *Biopolymers* **103,** 509–516 (2015).

61. Bernacchi, S., Henriet, S., Dumas, P., Paillart, J. C. & Marquet, R. RNA and DNA binding properties of HIV-1 Vif protein: A fluorescence study. *J. Biol. Chem.* **282,** 26361–26368 (2007).

62. Kapuscinski, J., Darzynkiewicz, Z. & Melamed, M. R. Interactions of acridine orange with nucleic acids. *Biochem. Pharmacol.* **32,** 3679–3694 (1983).

63. Naohisa Kure, Takayuki Sano, Shoji Harada, T. Y. Kinetics of the Interaction between DNA and Acridine Orange. *Bull. Chem. Soc. Jpn.* **61,** 643–653 (1988).

64. Wakelin LP, Creasy TS, W. M. Equilibrium constants for the binding of an homologous series of monofunctional and bifunctional intercalating diacridines to calf thymus DNA. *FEBS Lett.* **104,** 261–5 (1979).

65. Ihmels, H. & Otto, D. Intercalation of Organic Dye Molecules into Double-Stranded DNA. General Principles and Recent Developments. *Top Curr Chem* **258,** 161–204 (2005).

66. Wakelin, L. P. *et al.* Structural limitations on the bifunctional intercalation of diacridines into DNA. *Biochemistry* **17,** 5057–5063 (1978).

67. Haran, T. E. & Mohanty, U. The unique structure of A-tracts and intrinsic DNA bending. *Quarterly Reviews of Biophysics* **42,** 41-81, (2009).

68. Mitchell, J. S., Glowacki, J., Grandchamp, A. E., Manning, R. S. & Maddocks, J. H. Sequence-Dependent Persistence Lengths of DNA. *J. Chem. Theory Comput.* **13,** 1539–1555 (2017).

69. Nikolova, E. N., Bascom, G. D., Andricioaei, I. & Al-Hashimi, H. M. Probing sequence-specific DNA flexibility in A-tracts and pyrimidine-purine steps by nuclear magnetic resonance 13C relaxation and molecular dynamics simulations. *Biochemistry* **51,** 8654–8664 (2012).

70. Dršata, T. *et al.* Mechanical properties of symmetric and asymmetric DNA A-tracts: Implications for looping and nucleosome positioning. *Nucleic Acids Res.* **42,** 7383–7394 (2014).

71. Hud, N. V. & Plavec, J. A unified model for the origin of DNA sequence-directed curvature. *Biopolymers* **69,** 144–159 (2003).

72. Harteis, S. & Schneider, S. Making the bend: DNA tertiary structure and protein-DNA interactions. *Int. J. Mol. Sci.* **15,** 12335–12363 (2014).

73. Imae, T., Hayashi, S., Ikeda, S. & Sakaki, T. Interaction between acridine orange and polyriboadenylic acid. *Int. J. Biol. Macromol.* **3,** 259–266 (1981).

74. Kuruvilla, E., Joseph, J. & Ramaiah, D. Novel bifunctional acridine-acridinium conjugates: Synthesis and study of their chromophore-selective electron-transfer and DNA-binding properties. *J. Phys. Chem. B* **109,** 21997–22002 (2005).

75. Darzynkiewicz, Z. Differential staining of DNA and RNA in intact cells and isolated cell

nuclei with acridine orange. *Methods Cell Biol* **33,** 285–298 (1990).

76. Ichimura, S. Differences in the Red Fluorescence of Acridine Orange Bound to Single-Stranded RNA and DNA. *Biopolymers* **14,** 1033–1047 (1975).

**Supplementary Information**
**Characterization of the binding interactions between EvaGreen dye and dsDNA**

L. C. T. Shoute and G. R. Loppnow*
Department of Chemistry, University of Alberta, Edmonton, AB T6G 2G2 Canada

Hill analysis: To gain insight into the binding interaction between the duplex DNA (poly-$dA_{17}$·poly-$dT_{17}$) and EG, we have prepared and recorded the fluorescence spectra of solutions containing both dsDNA and EG. The traditional graphical representation of a binding isotherm is obtained by plotting the fractional saturation binding (θ) of ligand to the receptor, calculated as a function of the free ligand concentration present in the solution at equilibrium. Assuming the fluorescence intensity is linearly proportional to the number of bound EG to the duplex DNA, the measured fluorescence intensity can be used[1–5] to calculate the fraction of EG bound to duplex DNA as a function of free equilibrium EG concentration ($[EG]_{eq}$). The fluorescence intensity as a function of $[EG]_{eq}$ is shown in Figure 1S for the solution containing poly-$dA_{17}$·poly-$dT_{17}$ dsDNA and EG. The sigmoidal shape of the plot indicates cooperative binding of EG to dsDNA.

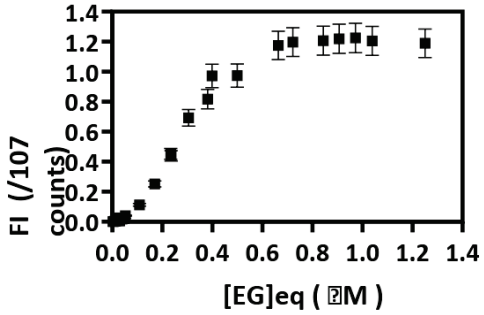

Figure 1S. Fluorescence intensity versus $[EG]_{eq}$ plot for intercalation of EG in 0.2 μM duplex poly-$dA_{17}$·poly-$dT_{17}$ (10 mM Tris, 1 mM EDTA, 10 mM NaCl, pH 7.5). The data points represent the average (point) and standard deviation (error bars) from 4 separate experiments.

The fraction of EG bound or fractional saturation (θ) can be found from the fluorescence intensity as follows:

$$\theta = \frac{F_{obs} - F}{F_{max} - F} = \frac{concentration\ of\ bound\ EG}{concentration\ of\ binding\ sites} \qquad (1)$$

Where $F_{obs}$ and F are the observed fluorescence intensity at 532 nm of EG in the presence and the absence of 0.2 μM duplex DNA, respectively, and $F_{max}$ is the maximum fluorescence attained at binding saturation. Figure 2S displays the binding isotherm obtained for the binding interaction of EG with duplex poly-$dA_{17}$·poly-$dT_{17}$.

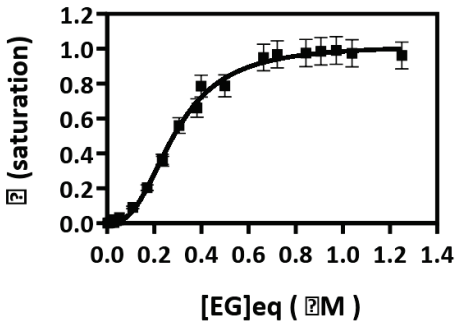

Figure 2S. Binding isotherm for the intercalation of EG into 0.2 μM duplex poly-$dA_{17}$·poly-$dT_{17}$ (10 mM Tris, 1 mM EDTA, 10 mM NaCl, pH 7.5). The data points represent the average (point) and standard deviation (error bars) from 4 separate experiments. The curve is the fit of the experimental data to the Hill equation (Eq. 5) using the parameters $K_a^m$ = (3.5±0.0) x$10^6$ and m = 2.7±0.2.

To quantify the binding of EG to dsDNA, a simple equilibrium model first introduced by Hill and co-workers[6–11] was used as follows:

$$\text{DNA} + \text{mEG} \rightleftharpoons \text{DNA•EG}_\text{m} \qquad (2)$$

$$K_d^m = \frac{[DNA]_{eq} \times [EG]_{eq}^m}{[DNA \bullet EG_m]_{eq}} \qquad (3)$$

In this model, the fractional saturation of the binding sites (θ) in duplex DNA available for occupation by the EG dyes is given by

$$\theta = \frac{m[DNA \bullet EG_m]_{eq}}{[DNA]_{eq,tot}} \qquad (4)$$

The fluorescence intensity from the dsDNA•$EG_m$ complex is proportional to the number of bound EG, and $[DNA]_{eq,tot}$ refers to the dsDNA concentrations. In this model, duplex DNA is described as a system with a one-dimensional array of binding sites. Substitution of Equation 3 into Equation 4 and rearrangement yields the sigmoidal form of the Hill equation describing the ligand binding isotherm,

$$\theta = \frac{[EG]_{eq}^{m}}{K_d^m + [EG]_{eq}^{m}} \quad (5)$$

Figure 2S shows that Equation 5 fits the experimentally observed isotherm with m=2.7, indicating positive cooperativity for the intercalation binding of EG into duplex poly-$dA_{17}$·poly-$dT_{17}$. Further, Equation 5 can be easily rearranged to the well-known linear forms of the Hill equation,

$$\frac{\theta}{1-\theta} = \frac{[EG]_{eq}^{m}}{K_d^m} \quad (6)$$

$$log\frac{\theta}{1-\theta} = m\ log[EG]_{eq} - m\ logK_d \quad (7)$$

Although the Hill equation can be used to determine binding parameters such as the affinity constant and the number of ligands bound to duplex DNA, it rarely correctly describes the binding interaction; the Hill model, as presented in Eq. 7, is linear only for two limiting cases, completely non-cooperative binding when m = 1 and infinitely cooperative binding where the binding of the first ligand imparts infinitely high affinity for the subsequent ligands, i. e. the contributions of the intermediate complexes or partially occupied sites (DNA•$EG_1$, DNA•$EG_2$,……DNA•$EG_{m-1}$) are negligible and the system is dominantly in the form of either DNA or the fully-bound DNA•$EG_m$ complex ("all-or-none" binding). Hence, the Hill model is useful only as a test for the deviation from a simple binding model and for detecting the presence of cooperativity (positive or negative) in the binding[6-11].

**References:**

1. Dragan, A. I. *et al.* Characterization of PicoGreen interaction with dsDNA and the origin of its fluorescence enhancement upon binding. *Biophys. J.* **99,** 3010–3019 (2010).
2. Paul, P. & Suresh Kumar, G. Thermodynamics of the DNA binding of phenothiazinium dyes toluidine blue O, azure A and azure B. *J. Chem. Thermodyn.* **64,** 50–57 (2013).
3. Dragan, A. I. *et al.* SYBR Green I: Fluorescence properties and interaction with DNA. *J. Fluoresc.* **22,** 1189–1199 (2012).
4. Ma-Ham, A. *et al.* Apoferritin-based nanomedicine platform for drug delivery: equilibrium binding study of daunomycin with DNA. *J. Mater. Chem.* **21,** 8700 (2011).
5. McMasters, S. & Kelly, L. A. Sequence-dependent interactions of cationic naphthalimides and polynucleotides. *Photochem. Photobiol.* **83,** 889–896 (2007).
6. Hill, A. V. The possible effects of the aggregation of the molecules of haemoglobin on its dissociation curves. *J. Physiol.* **40,** iv–vii (1910).
7. Cattoni, D. I., Chara, O., Kaufman, S. B. & Flecha, F. L. G. Cooperativity in binding processes: New insights from phenomenological modeling. *PLoS One* **10,** 1–14 (2015).
8. Eaton, W. A., Henry, E. R., Hofrichter, J. & Mozzarelli, A. Is cooperative oxygen binding by hemoglobin really understood? *Rend. Lincei* **17,** 147–162 (2006).
9. Gesztelyi, R. *et al.* The Hill equation and the origin of quantitative pharmacology. *Arch. Hist. Exact Sci.* **66,** 427–438 (2012).
10. Goutelle, S. *et al.* The Hill equation: A review of its capabilities in pharmacological modelling. *Fundam. Clin. Pharmacol.* **22,** 633–648 (2008).
11. Lolkema, J. S. & Slotboom, D.-J. The Hill analysis and co-ion-driven transporter kinetics. *J. Gen. Physiol.* **145,** 565–74 (2015).